Simulation of Electron Hop Funnel Hysteresis

Marcus Pearlman, *Student Member, IEEE*, Tyler Rowe, *Student Member, IEEE*, and Jim Browning, *Senior Member, IEEE*

***Abstract*— Insulating funnels, called electron hop funnels, use secondary electron emission and an electric field created by an electrode to transport current through the device. The surface charge along the funnel wall self-adjusts to get unity-gain transmission. Electron hop funnels allow increased control over the spatial and energy uniformity of the transmitted beam from a field emitter array. Measurements performed on the relationship between transmission through the device and the electrode voltage has shown hysteresis. To better understand the origin of the hysteresis, simulations have been performed using the particle trajectory code Lorentz 2E. The simulations reveal two very important mechanisms that define the transmission through the funnel. The simulations also show that hysteresis is a fundamental characteristic of hop funnels.**

***Index Terms*— Electron beams, electron emission, surface charging, vacuum microelectronics.**

I. Introduction

FIELD emission arrays (FEAs) have many desirable qualities as an electron source [1], [2]. Electron hop funnels are devices that have been proposed to improve FEA performance by increasing uniformity and providing protection [3], [4]. With these benefits, hop funnels can aid in the integration of FEAs in microwave vacuum electron devices (MVEDs). Hop funnels use secondary electron emission to transport current through the device.

Hop funnels are holes, funnels, or slits fabricated into an insulating material. A cross-sectional diagram of the funnel studied in this paper is shown in Fig. 1. The narrow end (exit) is surrounded by an electrode, referred to as the hop electrode, and the wide end (entrance) is where the electrons enter the funnel. Electrons are emitted up and into the funnel, are pulled up by the electric field created by the hop electrode, and hop along the funnel wall via secondary electron emission. This hopping mechanism is referred to as electron hopping transport [5].

When the potential of the hop electrode is high enough, the amount of current leaving the funnel is the same as the current injected into the funnel; this operating point is known as unity gain [5]. Fig. 2 shows the trajectories of a hop funnel at unity gain as simulated by the Lorentz 2E software [6]. When the potential of the hop electrode is too low, the electric field in the funnel is not sufficient to transport the current on the wall, the funnel wall will charge negative, and many of the electrons will be turned back toward the cathode, as shown in Fig. 1. The relationship between the transmitted current and the voltage on the hop electrode (*I–V* characteristic) allows a method to study the electron transport mechanism and the secondary electron characteristics of the material. Current methods to measure secondary emission yield (SEY) of insulators need to account for the charging of the insulator, and the setup is not operated in steady state [7], [8]. These methods can be difficult to implement. The correlation between SEY and the steady-state operation of hop funnels makes them an attractive possibility for measuring SEY.

The use of hop funnels in field emission displays has shown a significant improvement in spatial and energy uniformity in the resulting electron beam [9]. The *I–V* characteristic has been measured and simulated [3]. Although not mentioned explicitly, the measurements show a hysteresis [3]. Ramping the voltage from low to high yields different results than ramping from high to low.

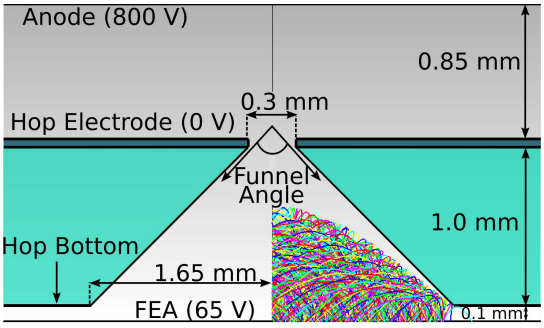

Fig. 1. Hop funnel diagram showing the dimensions used in this paper and showing the repelled electron trajectories when using a low hop electrode voltage from Lorentz 2E.

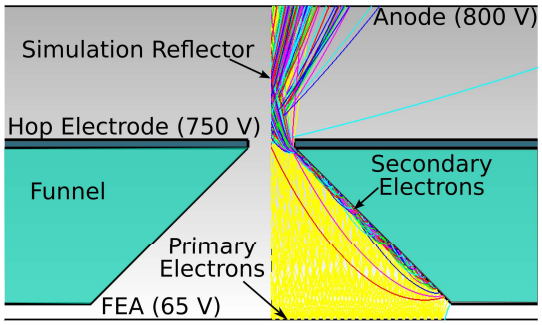

Fig. 2. Hop funnel diagram showing the operation of the funnel during unity gain from Lorentz 2E.

Manuscript received October 9, 2012; revised April 17, 2013; accepted June 26, 2013. Date of publication July 24, 2013; date of current version August 7, 2013. This work was supported in part by the U.S. Air Force Office of Scientific Research under Grant FA9550-08-1-0396 and the Electrical and Computer Engineering Department at Boise State University.

The authors are with the Electrical and Computer Engineering Department, Boise State University, Boise, ID 83725 USA (e-mail: marcuspearlman@u.boisestate.edu; tylerrowe@u.boisestate.edu; jimbrowning@boisestate.edu).

Color versions of one or more of the figures in this paper are available online at http://ieeexplore.ieee.org.

Digital Object Identifier 10.1109/TPS.2013.2271998

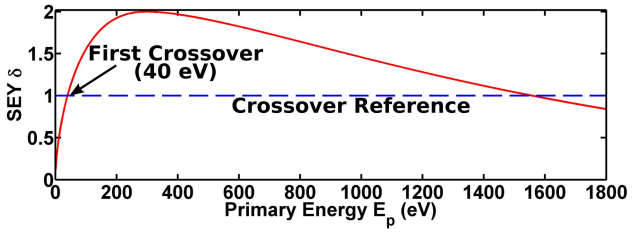

Fig. 3. Vaughan secondary electron emission curve [13] with $\delta_{\max} = 2$ and $E_{\max} = 300$ as used in the Lorentz 2E simulation.

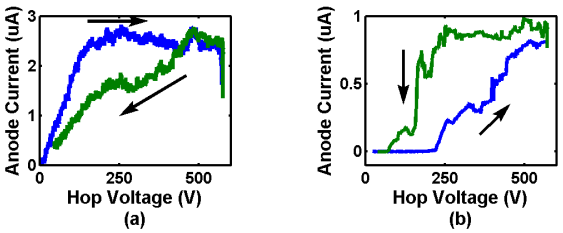

Fig. 4. Range of results observed for hop funnels. (a) is a 90° funnel with a metal hop bottom. (b) is a 90° funnel without a metal bottom [10].

Finding the cause of the hysteresis is the focus of this paper. Three different possibilities of the hysteresis are proposed: 1) charging of the FEA cathode itself; 2) charging on the hop bottom; or 3) hysteresis is a fundamental characteristic of the funnel operation. Hypotheses 1 and 2 are discussed in [10]. To test hypothesis 3, simulations were implemented with Lorentz 2E to recreate the hysteresis observed experimentally. The focus of this paper is on the simulations to recreate the hysteresis.

II. Theory of Operation

The operation of the hop funnel relies on secondary electron emission and the electron-hopping transport mechanism. These phenomena are briefly described here.

A. Secondary Emission Yield

The number of secondary electrons produced from an electron collision with a material depends primarily on the energy of the primary electron. There are many formulas that have been developed over the years [11]–[13] to describe this relationship, but the model used in Lorentz 2E is the Vaughan model [13].

The two physically meaningful parameters that define the SEY characteristics of the material are the maximum secondary electron yield, $\delta_{\max}$, and the energy at which the maximum occurs, $E_{\max}$.

The Vaughan model is not described in detail here, but a plot of an example curve with $\delta_{\max} = 2$ and $E_{\max} = 300$ is shown in Fig. 3. The crossover reference line is also suggested to show the energies where an electron produces one secondary electron. There are two points at which this occurs, but the first crossover point is the operating point important to electron hop funnels and is labeled in the figure. The crossover reference is only for SEY and does not include backscattered electrons. In the context of electron hop funnels, the crossover reference would be where an electron produces one offspring because of all mechanisms of which backscatter and secondary electron emission are the two main mechanisms. The dominant mechanism in electron-hopping transport is secondary electron emission, and backscatter has little effect [14].

B. Electron-Hopping Transport

Electron-hopping transport is the mechanism by which electrons transport across an insulator via secondary electron emission. To initiate electron-hopping transport, a strong electric field both lateral and perpendicular to the wall is needed [5]. Electrons that strike the wall may produce secondary electrons. These secondary electrons are pulled along the wall and can also strike the wall. This collision can create more secondary electrons, and the cycle continues until no new secondary electrons are generated or until the electrons exit the funnel.

To sustain electron-hopping transport, the average total electron yield through the geometry must be equal to unity. With a favorable electric field, the electron-hopping mechanism self-regulates the surface charge along the wall to control the energies of the incoming electrons to maintain unity [5]. The average landing energy at which electrons collide with the wall corresponds to the first crossover energy of the material. With an unfavorable electric field in the funnel, negative charge accumulates on the wall, and will reach equilibrium as this accumulated charge repels any incoming electrons back to the cathode, as shown in Fig. 1. The examples of no transmission and unity gain shown in Figs.1 and 2 are the two extremes of whether transport occurs or not, but there can be a hybrid of the two where a portion of the wall can sustain transport and another portion may not. Examples of these are shown later.

There are two criteria that determine if the electric field is favorable or not: 1) primary electrons must have an energy above the first crossover when they collide with the wall and 2) the electric field must be sufficient to pull secondary electrons up the wall. The justification of these two criteria is one of the main themes of this paper and is discussed in detail.

III. Experimental Hysteresis

In [10], experiments were performed with funnels made from low-temperature cofired ceramic (LTCC) [15] to show the hysteresis in the *I–V* curves and to rule out charging on the hop bottom as the fundamental source. The experiment measured the transmitted current versus the hop electrode voltage for voltages from 0 to 550 V.

The *I–V* measurement results show many different shapes and two *I–V* curve examples, which represent a good range of the results observed, are shown in Fig. 4. The total emitted current is unknown so the plots show unnormalized data. Many curves show a knee (a sharp transition from unity gain to no transmitted current) and linear variations (a relatively slow transition from no transmission to transmission). The slight bumps in the curve are often observed, and are not considered noise because they are repeatable within the setup. The ramp-up curve may occur at higher voltages than the ramp-down or the opposite.

With the wide range of results, little can be concluded about the hop funnel operation except that hysteresis exists. Each experiment performed was attempted to be identical to each other; however, slight changes are unavoidable and are the cause of the wide variation. The emissive properties of the FEA, charging of the FEA, voltage of the FEA, the initial electron energy, charging of the hop bottom, the SEY characteristics of the insulator, position of the funnel on top of the FEA, and stray current all contribute to the shape of the *I–V* curve. Many of these variables cannot be controlled with the current experimental setup; therefore, to gain insight, simulations were performed.

IV. Simulation Setup

To simulate the electron hop mechanism, Lorentz 2E was used.

A. Lorentz Model Summary

The simulation model is shown in Figs. 1 and 2. The FEA is represented by an emitter boundary adjacent to a potential/collecting boundary. Electron rays are emitted from the emitting boundary with a typical directional distribution characteristic of FEAs [3]. The initial energy of each ray, W_p, is constant. The potential/collector boundary represents the potential of the gate of the FEA, V_{gate}. Each ray in Figs. 1 and 2 represents a number of electrons.

The funnel wall is represented by a secondary emitting boundary. The dielectric constant of the funnel region is 7.8 for LTCC. The secondary emission yield characteristics are modeled using the semiempirical model devised by Vaughan [13]. The Vaughan model in Lorentz 2E uses two inputs: the maximum SEY, $\delta_{\max}$, and the energy where the maximum yield occurs, $E_{\max}$. Lorentz 2E supplies an input for the average energy of the secondary electron, $W_{\text{avg}} = 5\,\text{eV}$. To reduce simulation time, the angle of the emitted secondary electrons is not random, but the first secondary electron is emitted normal to the surface, and the next two are emitted at an angle of $\pm 45^\circ$ from the normal. To model the charging of the funnel surface, the secondary emitting boundary of the funnel wall is discretized into 300 segments. The net charge deposited by the electrons is then calculated for each segment and interpolated with the neighboring segment. The electrodes are modeled by a potential and collector boundary. The model is rotationally symmetric about the simulation reflector axis.

To more accurately describe the emission angle, a cosine distribution should be used [16]. To use this probabilistic model, a significant number of rays are needed to get consistent results. It is impractical in the Lorentz model to add the needed rays because this will increase the simulation time at least 2–3 times. The electron transport mechanism will still occur with the nonrandom distribution of emitted angles.

A boundary element method [6] is used to calculate the electric field. This method includes surface charge, and for the electron currents used in the simulation and experiment, space charge can be ignored. The electron ray trajectories are tracked using a time-doubling adaptive step fifth-order Runge–Kutta method referred to as RK5 [17]. The timesteps of each ray motion are independent of the other rays and usually in the order of 10^{-11} s.

To simulate the surface charge model to steady state, a time step method is used. The charge-per-ray, Q, is determined from three parameters: the number of rays N, total emission current I_{T}, and the iteration timestep Δt. The charge-per-ray is $Q = I_{\text{T}} \cdot \Delta t / N$. The iteration timestep is independent of the electron trajectory timestep of each ray used in the Runge–Kutta method. The choice in the charge-per-ray and the number of rays greatly affects the stability of the simulation and the simulation time. An extensive study was performed to determine these parameters [3], and the parameters used in this paper are derived from that study to minimize simulation time and minimize instabilities: $N = 192$ rays, $I_{\text{T}} = 1\mu\text{A}$, and $\Delta t = 5\ \mu\text{s}$, which correspond to $Q = 2.6 \times 10^{-14}$ C/ray.

The simulation flow is as follows. The electric field is calculated for the domain. Then, the primary electron rays are launched from the emitting boundaries of the FEA and tracked. The electron rays are tracked until they strike a collector or a secondary emitting boundary. After all of the primary electron rays are launched and tracked, the secondary electron rays are launched from the secondary electron boundaries and tracked. These secondary electron rays are tracked until they hit either a collecting or secondary emitting boundary. This process repeats until there are no more secondary electron rays produced from a collision. This is the point at which the surface charge on the secondary emitting boundaries and the electric field are updated. This cycle constitutes one surface charge iteration. Many of these iterations (300–500) are performed to reach the steady-state solution at which the hop exit current is approximately constant.

B. Simulation Procedure

To simulate the *I–V* hysteresis, a ramping of the hop voltage was performed using discrete voltage steps with the initial condition of the steady-state conditions for the previous voltage step simulation. The voltage step procedure is outlined as follows.

1) Initial uncharged wall simulation at either $V_{\text{hop}} = 0$ V or $V_{\text{hop}} = 650$ V.
2) After the anode current reaches a relative steady state, save the wall surface charge.
3) Increment the hop voltage to the new value.
4) Import the steady-state surface charge from the previous voltage simulation.
5) Run the simulation with the new voltage and the surface charge from the previous step.
6) Repeat Steps 2−5 for the desired voltage ramp.

V. Simulation Results

The secondary electron characteristics are unknown for LTCC. Lester *et al.* [3] found that $\delta_{\max} = 2$ and $E_{\max} = 500$ eV, which correspond to a 70-eV first crossover, closely resembled experimental *I–V* curves. It should be noted that a continuum of $\delta_{\max}$ and $E_{\max}$ values yield the same first crossover and yield the same *I–V* curves. The new modeling results, using the ramping of the hop voltage, found that the

TABLE I
SUMMARY OF THE SIMULATION PARAMETERS

Name	First Crossover	V_{gate} [V]	E_i [eV]	Critical Voltage Contour	δ_{max}	E_{max} [eV]
Case 1	40 eV	65	55	50 V	2	300
Case 2	70 eV	65	55	80 V	2	500
Case 3	70 eV	95	85	80 V	2	500

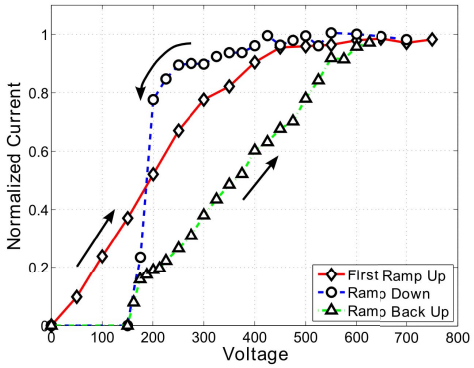

Fig. 5. Simulated *I–V* curves showing a full ramp-up–down-up procedure for case 1.

70-eV first crossover did not match experimental results. It was estimated that a 40 eV first crossover would shift the knee to a lower voltage. $\delta_{\max} = 2$ and $E_{\max} = 300$ eV were chosen to generate this first crossover and it resembled experimental results better.

Three different cases were simulated and the parameters are summarized in Table I. Two different first crossovers were simulated: 40 eV and 70 eV. The discrepancy in the observed *I–V* curves between cases 1 and 2 prompted the simulation of case 3 with the modified gate voltage and initial electron energy as will be discussed later. Fig. 5 shows the resulting *I–V* curves of ramping up, down, and then back up the hop voltage for case 1.

A. 40-eV First Crossover Ramp-Up

The ramp-up curve shows a roughly linear behavior until the current becomes saturated. To visualize this behavior, the electron trajectories and voltage contours for $V_{\text{hop}} = 50$, 350, and 750 V are shown in Fig. 6. These voltage contours were gathered before the first iteration at each voltage step (i.e., the steady-state surface charge of the previous voltage step and the hop voltage of the current step). The trajectories are at steady state of the corresponding voltage step.

The linear behavior during the ramp-up is caused by two opposing mechanisms: 1) incremental negative surface charging on the funnel wall and 2) electric field penetration through the funnel exit. Starting from the first simulation $\left(V_{\text{hop}} = 0\,\text{V}\right)$, the energy at which the primary electrons hit the wall is below the first crossover. Fewer than one secondary electron is produced from each primary along the entire wall. This causes the wall to charge negative, repelling the incoming electrons, and causing the primary electrons to collide with even less energy. Eventually, the wall charges negative to the point where no electrons collide with the wall, and all electrons are repelled back to the FEA. On the next voltage

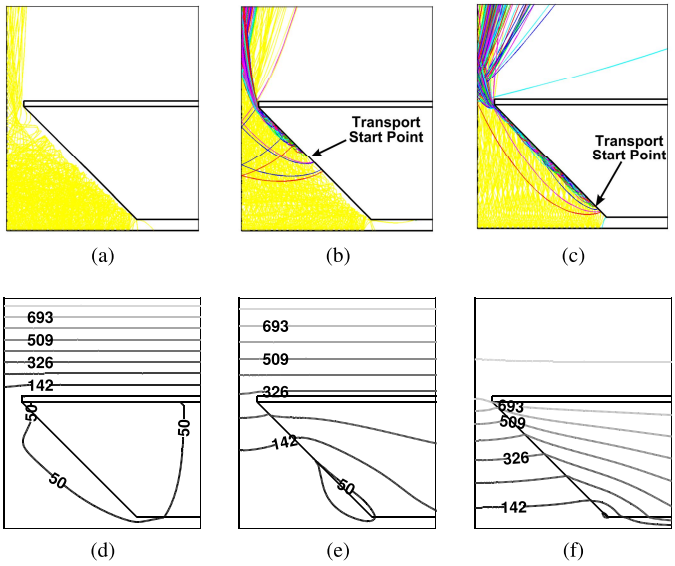

Fig. 6. Plots of the steady-state electron ray trajectories and the corresponding initial condition voltage contour plots for a range of hop voltages for case 1 ramp-up-first. The primary rays emitted from the FEA are yellow and the secondary rays are shown in other colors. (a) The ray trajectories with $V_{\text{hop}} = 50$ V. (b) The ray trajectories with $V_{\text{hop}} = 300$ V. (c) The ray trajectories with $V_{\text{hop}} = 750$ V. (d) The voltage contours with $V_{\text{hop}} = 50$ V. (e) The voltage contours with $V_{\text{hop}} = 300$ V. (f) The voltage contours with $V_{\text{hop}} = 750$ V.

step, the accumulated surface charge from the previous step prevents this new generation of electrons from colliding at energies above the first crossover. The wall continues to charge negative. Fig. 6(d) shows a good example of the effect of the negatively charged wall. This mechanism, by itself, would prevent current from ever transmitting through the funnel, but this mechanism is counteracted by electric field penetration through the funnel exit.

On each increasing voltage step, the electric field penetrates farther into the funnel exit. As the hop voltage is increased from 0 to 50 V, the electric field penetrates the funnel opening enough, shown in Fig. 6(d), to allow some of the primary electrons through, shown in Fig. 6(a). The next voltage step, the electric field penetrates enough to cause electron transport to take place along the funnel wall immediately near the exit. Each increment in hop voltage allows the electric field to penetrate into the funnel for allowing electron transport to occur farther and farther down the wall. Fig. 6(b) and (e) shows the effects of the two mechanisms occurring simultaneously. The region of negative charged space near the funnel entrance is referred to here the charge sink region. The charge sink region forms an electric field barrier that prevents electrons from hitting the wall at an energy above the first crossover. The effect of the charge sink barrier can be seen by the corresponding trajectories shown in Fig. 6(b). At the highest voltage of the ramp-up, the charge sink region is virtually nonexistent, shown in Fig. 6(f), and secondary electron transport takes place on almost all of the wall except for near the funnel entrance, as shown in Fig. 6(c).

The point at which electron transport occurs in this example is determined by the intersection of the 50 V contour line, labeled critical voltage contour in Table I. The 50 V contour line is labeled in the contour plots and can be compared with

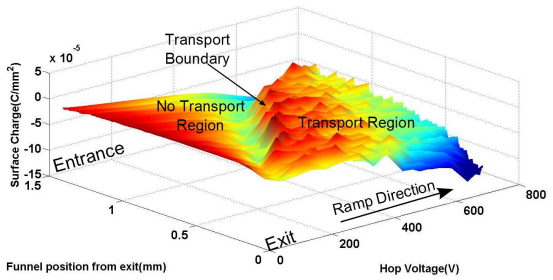

Fig. 7. Surface charge density evolution during the ramp-up for case 1. The no transport region describes the portion of the wall where no electron transport is taking place. The transport region describes where electron transport is taking place. The transport boundary corresponds to the transport start point on the funnel wall.

the transport start point in Fig. 6. This contour line corresponds to the potential at which primary electrons can hit the wall with energies above the first crossover $(E_p = 40\ \text{eV})$. The initial electron energy of the primary electron is 55 eV, which is emitted from a 65 V potential. As the electron moves from the 65 to 50 V contour, 15 eV of energy is lost. The resulting energy is 40 eV, which corresponds to the first crossover of the secondary electron yield curve. Each hop voltage increment causes a linear movement in the 50 V contour, which then causes a linear movement in the electron transport start point; hence, a linear gain in transmitted current is observed.

Fig. 7 shows the surface charge density along the wall at each hop voltage throughout the ramp-up. This type of view shows how the surface charge in the funnel transitions to electron transport. The no transport region shows a continuous negative charging because of the incremental surface charging mechanism. The negative charging is ended by a sharp positive charging at the transport boundary because of electron transport starting to take place. The positive charging at this point is caused by secondary electrons readily leaving the local region, thus charging the region positive to reach unity. The transport boundary moves down the funnel wall as the electric field penetrates the funnel. The transport region also shows a continuous negative charging. Electron transport continues to take place, but to keep the SEY at unity, the wall charges more negative.

This sharp positive charging at the transport boundary because of initiation of electron transport causes the region in the funnel to be in a new state. With electron transport occurring along the wall, it becomes more difficult to stop the mechanism and sets up the funnel for a different behavior during the following ramp-down.

B. 40-eV First Crossover Ramp-Down

The ramp-down shows a fairly constant transmission current until a knee at $V_{\text{hop}} = 200$ V. The slight loss in current before the knee (750–200 V) is caused by the movement of the 50 V contour line. To explain this behavior, the trajectories along with the corresponding voltage contours are shown for $V_{\text{hop}} = 525$, 200, and 175 V in Fig. 8.

As the hop voltage is decreased, secondary electron transport continues to take place along the majority of the wall except for a region near the funnel entrance. This local charge

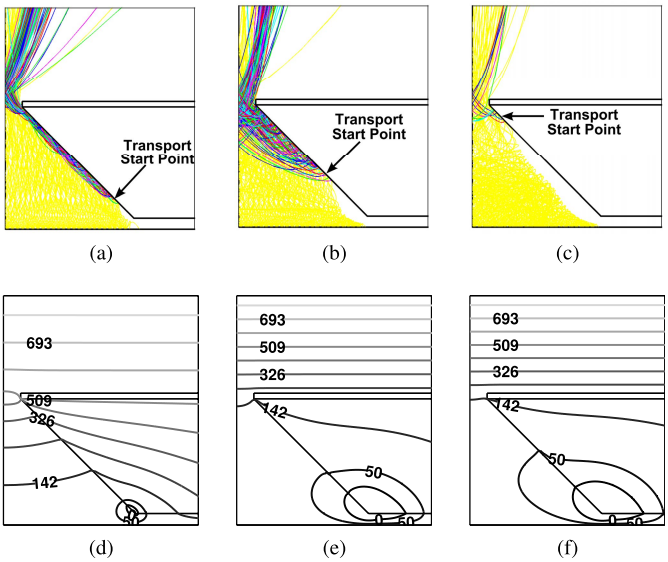

Fig. 8. Plots of the steady-state electron ray trajectories and the corresponding initial condition voltage contour plots for a range of hop voltages for case 1 ramp-down. The primary rays emitted from the FEA are yellow and the secondary rays are shown in other colors. (a) The ray trajectories with $V_{\text{hop}} = 525$ V. (b) The ray trajectories with $V_{\text{hop}} = 200$ V. (c) The ray trajectories with $V_{\text{hop}} = 175$ V. (d) The voltage contours with $V_{\text{hop}} = 525$ V. (e) The voltage contours with $V_{\text{hop}} = 200$ V. (f) The voltage contours with $V_{\text{hop}} = 175$ V.

sink region was left behind during the last voltage step of the ramp-up. As the hop voltage is lowered, the relatively small amount of negative charge in the charge sink region has little effect on the movement of the 50 V contour, as shown in Fig. 8(d) and (e). If there were more charge in the charge sink region, the effect on the voltage contours would be greater. In addition, the slow movement of the critical contour can be attributed to choice in the gate voltage of the FEA, and is discussed in more detail in the explanation of cases 2 and 3.

Lowering the hop voltage in this case does have a large effect on the voltage gradient in the center of the funnel. Lowering the hop voltage from 700 to 200 V, the electric field in the center of the hop funnel is decreased, but it maintains a strong enough field to pull the secondary electrons up the funnel to gain at least 40 eV of energy. Fig. 8(e) shows the weak voltage gradient right before the knee, and Fig. 8(b) shows the resulting trajectories. The secondary electrons in this figure are pulled much farther away from the wall at this hop voltage, but they still gain enough energy in the trajectory to maintain electron transport. The critical voltage step from 200 to 175 V is when the voltage gradient becomes insufficient, and the majority of the negative charging along the wall occurs. Secondary electrons travel laterally across the funnel, are reflected by the simulation reflector, and land very close to where they were created. Little energy is gained during this trajectory, and the electrons deposit their charge on the funnel wall. This large negative charging causes the movement of the hopping transport point up the funnel wall, resulting in the trajectories shown in Fig. 8(c), and the spatial change in this transport point is much greater than the initial movement of the 50 V contour shown in Fig. 8(f).

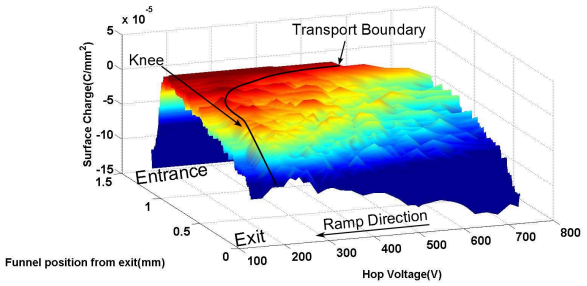

Fig. 9. Surface charge density evolution during a ramp-down for case 1.

Fig. 9 shows the surface charge density evolution throughout the ramp-down. As the hop voltage is lowered, the surface charge becomes less negative. This charging is due to electron transport self-regulating the surface charge to maintain the SEY at unity. The transport boundary moves up the funnel slowly at first, but then moves substantially at 175 V. In the region before the knee, where the electron transport point moves because of the movement of the 50 V contour, a little negative charging is observed. At the knee, an increased negative charging is observed at the transport boundary. This is the point at which the electric field is insufficient to maintain electron transport. This negative charging puts the funnel into a new state and defines the behavior in the following ramp-back-up.

C. 40-eV First Crossover Ramp-Back-Up

For brevity, no figures are presented to describe the behavior of the ramp-back-up, but the mechanisms that describe the shape are very similar to the first ramp-up. The main difference between the ramp-back-up and the first ramp-up is the initial surface charge left behind by the ramp-up and ramp-down. The linear behavior is observed but at a different starting point and with an initial steep increase in current. The initial jump in current from 150 to 175 V is from primaries being allowed to pass through. The linear behavior thereafter is due to the incremental surface charging along with field penetration.

D. 70-eV First Crossover

The ramp-up-down-up procedure was also performed on a funnel with a 70-eV first crossover. The same initial energy, $W_p = 55$ eV, and gate voltage, $V_{gate} = 65$ V, was used in case 2. The *I–V* curves for case 2 are shown in Fig. 10. The first ramp-up shows a linear variation, which resembles the first ramp-up in case 1. The explanation for the linear variation in the ramp-up in case 2 is the same as for case 1. The ramp-up in case 2 has a more shallow slope because of the larger negative surface charge acquired because of the higher first crossover. The ramp-down is always negative sloping with a slight knee. The shape of the ramp-down in case 2 deviates greatly from case 1 and causes the ramp-back-up to overlap the curve. The shape of the ramp-down curve is due to the large movement of the critical voltage contour on each voltage step.

The contour line that corresponds to the potential at which primary electrons can hit the wall with energies above the first crossover $(E_p = 70\,\text{eV})$ is the 80 V contour. The initial

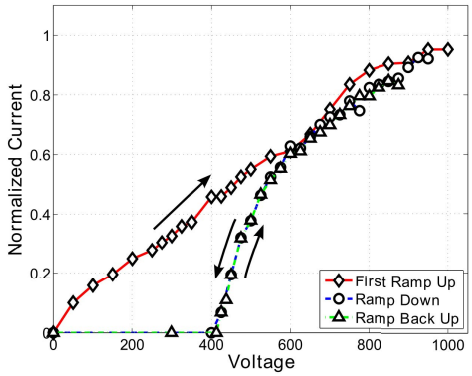

Fig. 10. Simulated *I–V* curves showing a full ramp-up–down-up procedure for case 2.

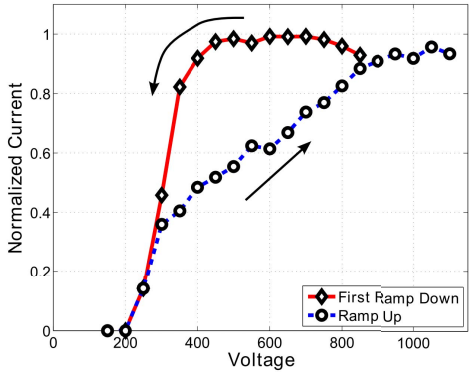

Fig. 11. Simulated *I–V* curves showing a ramp-down-up procedure for case 3.

electron energy of the primary electron is 55 eV, which is emitted from a 65 V potential. As the electron moves from the 65 to 80 V contour, 15 eV of energy is gained. The resulting energy is 70 eV, which corresponds to the first crossover of the secondary electron yield curve. During the ramp-down, the movement of this 80 V contour line is greater than observed in case 1 on each step, and the transport start point moves with it. On each voltage step, a large movement of the 80 V contour line is observed and eventually reaches the funnel exit. This larger movement of the 80 V contour line does not allow for a sudden negative charging because of a weak electric field, as was observed for case 1.

One of the main reasons why the critical voltage contour in case 2 moves differently than the critical voltage contour of case 1 is because of the gate voltage and the initial electron energy. By changing the initial electron energy from 55 to 85 eV and by changing the gate voltage from 65 to 95 V (case 3), the critical voltage contour is still the 80 V contour, but 15 eV of energy is lost in the trajectory. Fig. 11 shows the resulting *I–V* curve with the new initial energy and gate voltage. To save time, no ramp-up was simulated and only the ramp-down and then ramp-back-up. Preceding the ramp-down by a ramp-up has a little effect on the outcome of the ramp-down curve as long as the unity gain is achieved [18]. This may not necessarily be true all the time depending on the geometry and the max hop voltage in the ramp, but with the modest hop voltages presented here, the difference is minimal.

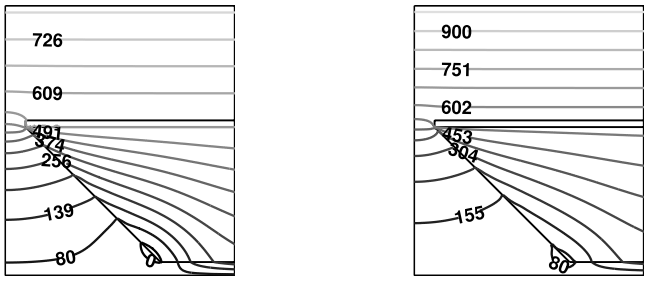

(a) (b)

Fig. 12. Voltage contours, with $V_{\text{hop}} = 550$ V during the ramp-down for (a) case 2 and (b) case 3.

The *I–V* curves shown in Fig. 11 now resemble the *I–V* curves in Fig. 5. The mechanisms that define the curves in case 3 are the same as case 1. From 800 to 350 V during the ramp-down, the shape is defined by the slight movement in the 80 V contour. From 325 to 200 V, the weak electric field gradient charges the wall negatively. The difference in shapes from Figs. 10 and 11 are due to the fact that the initial conditions of the electron source move the 80 V contour differently.

Fig. 12 shows the contours during a ramp-down of cases 2 and 3. Notice in Fig. 12(a), the 80 V contour spans the funnel. In the absence of charge, the voltage contours are determined by the boundaries (the gate and hop electrodes). By choosing the gate voltage to be 65 V, as in case 2, the 80 V contour lies between the gate and the hop electrode during the first iteration and thereafter. Decreasing the hop voltage decreases the electric field in the funnel region, which will have a large effect on the movement of the 80 V contour. With the gate voltage at 95 V and the absence of surface charge, the 80 V contour does not exist during the first iteration. The only way for the 80 V contour to exist, by Poisson's equation for electrostatics, is to have negative charge on the funnel wall. By changing the voltage of the hop electrode, the 80 V contour is affected little. The movement of the 80 V contour is affected more by the surface charge. By choosing the boundary conditions of case 3, the 80 V contour only appears after a few iterations by accruing some surface charge. The charge sink region is very small, as shown in Fig. 12(b), and grows very slowly. The slow contour movement during the ramp-down allows for the second mechanism, the weak electric field, to take over and cause sudden negative charging and thus a knee in the *I–V* characteristic. The sudden negative charging puts the funnel in a new state and sets up the following ramp-up for linear behavior, as seen in case 1.

VI. Conclusion

The transmission through the funnel is a result of the percentage of the wall that sustains electron transport. To initiate electron transport in a region, two conditions must be met at the wall surface: 1) primary electrons must have an energy above the first crossover and 2) the electric field must be sufficient to pull the secondary electrons up the wall. These two conditions alone define the behavior of electron transport. The initial electron energy and the gate voltage determine the critical voltage contour. The location of this critical voltage contour affects both mechanisms 1 and 2. By creating the conditions that prevent the movement of the critical voltage contour, a knee is observed and promotes hysteresis. By allowing the critical voltage contour to move with the hop voltage, no knee is observed and little hysteresis is observed.

The simulated hysteresis and curve shapes are not identical to the experimental data, but the simulation generated some of the experimental scenarios by modifying only the gate voltage, initial electron energy, and the first crossover. The shape of the curves depends on many variables included in the entire setup and it is likely that they will affect the location of the critical voltage contour and create many different shapes of the curves.

The dependence of the transport mechanism on the first crossover allows a new method to study secondary electron yield of insulators. Currently, measuring the SEY of insulators is difficult [7], [8]. Operating a hop funnel circumvents the charging problems in other experiments because of the self-adjusting surface charge mechanism inherent in the operation. Determining the first crossover point with high accuracy using hop funnels may be possible and determining other secondary electron information may also be possible. For example, the difference in locations of the knee during the ramp-down of cases 1 and 3 shown in Figs. 5 and 11, are indications of a correlation between the first crossover and the transmission characteristics of the funnel. By determining the correlation between full transmission of the funnel and the first crossover point, one can estimate the continuum of $\delta_{\max}$ and $E_{\max}$ parameters. By either different geometries of funnels or by another experiment entirely, one could pin down $\delta_{\max}$ and/or $E_{\max}$ and generate the whole curve with the Vaughan model. Of course, this method is only as good as the model for predicting other points on the curve. It may be possible to measure other points on the curve using temporal measurements of the funnel, measuring the electron energy distribution leaving the funnel, or by measuring the charge distribution along the funnel wall. This, of course, can increase the difficulty of the measurements to the order of existing methods, but it is a different method that may be found to be more accurate. There are many possibilities of SEY measurement, but only by understanding the *I–V* curves, we can obtain accurate SEY characteristics of materials using hop funnels. The difficulty in characterizing the *I–V* relationship of hop funnels is apparent in this paper, but more consistent experiments will overcome these difficulties.

Hysteresis of the hop funnels may not be that important when using them in MVEDs. In many applications, the hop funnel will only be used in the unity-gain regime. In this context, hysteresis is irrelevant. Studying the hysteresis, however, will help determine the limitations of hop funnels and may yield a new way to use them.

References

[1] I. Brodie and P. Schwoebel, "Vacuum microelectronic devices [and prolog]," *Proc. IEEE*, vol. 82, no. 7, pp. 1006–1034, Jul. 1994.

[2] D. Temple, "Recent progress in field emitter array development for high performance applications," *Mater. Sci. Eng. R, Rep.*, vol. 24, no. 5, pp. 185–239, Jan. 1999.

[3] C. Lester, J. Browning, and L. Matthews, "Electron-hop-funnel measurements and comparison with the Lorentz-2E simulation," *IEEE Trans. Plasma Sci.*, vol. 39, no. 1, pp. 555–561, Jan. 2011.
[4] L. Min, Z. Xiaobing, L. Wei, Z. Hongping, and W. Baoping, "Transverse energy distribution analysis in a field emission element with an insulator funnel," *Nuclear Instrum. Methods Phys. Res. Section B, Beam Interact. Mater. Atoms*, vol. 234, no. 3, pp. 210–218, Jun. 2005.
[5] B. Hendriks, G. van Gorkom, N. Lambert, and S. de Zwart, "Modes in electron-hopping transport over insulators sustained by secondary electron emission," *J. Phys. D, Appl. Phys.*, vol. 30, no. 8, pp. 1252–1264, Apr. 1997.
[6] (2013). *Integrated Engineering Software* [Online]. Available: http://www.integratedsoft.com/
[7] X. Meyza, D. Goeuriot, C. Guerret-Piécourt, D. Tréheux, and H.-J. Fitting, "Secondary electron emission and self-consistent charge transport and storage in bulk insulators: Application to alumina," *J. Appl. Phys.*, vol. 94, no. 8, pp. 5384–5392, Aug. 2003.
[8] E. R. B. Adamson, "Secondary electron emission coefficient from lexan: The low energy crossover," Ph.D. dissertation, Dept. Doctor Philosophy, Texas Tech Univ., Lubbock, TX, USA, May 1993.
[9] R. Tuck, W. Taylor, M. Waite, H. Bishop, R. Riggs, and J. Browning, "The pFED—A viable route to large field emission displays," in *18th IVNC Tech. Dig.*, Jul. 2005, pp. 80–81.
[10] T. Rowe, M. Pearlman, and J. Browning, "Hysteresis in experimental I-V curves of electron hop funnels," *J. Vac. Sci. Technol. B*, to be published.
[11] E. M. Baroody, "A theory of secondary electron emission from metals," *Phys. Rev.*, vol. 78, no. 6, pp. 780–787, Jun. 1950.
[12] R. G. Lye and A. J. Dekker, "Theory of secondary emission," *Phys. Rev.*, vol. 107, no. 4, pp. 977–981, Aug. 1957.
[13] J. Vaughan, "A new formula for secondary emission yield," *IEEE Trans. Electron Devices*, vol. 36, no. 9, pp. 1963–1967, Sep. 1989.
[14] B. H. W. Hendriks, G. G. P. van Gorkom, A. T. M. H. van Keersop, N. Lambert, and S. T. De Zwart, "Dynamical behavior of electron hop transport over insulating surfaces," *J. Appl. Phys.*, vol. 85, no. 3, pp. 1848–1856, Feb. 1999.
[15] (2001). *DuPont 951 Grean Tape Product Description* [Online]. Available: http://www2.dupont.com/MCM/en_US/assets/downloads/prodinfo/951LTCCGreenTape.pdf
[16] H. Seiler, "Secondary electron emission in the scanning electron microscope," *J. Appl. Phys.*, vol. 54, no. 11, pp. 1–18, Jul. 1983.
[17] W. H. Press, S. A. Teukolsky, W. T. Vetterling, and B. P. Flannery, *Numerical Recipes 3rd Edition: The Art of Scientific Computing*. Cambridge, U.K.: Cambridge Univ. Press, 2007.
[18] M. Pearlman, "Investigation of the current transmission hysteresis in electron hop funnels," M.S. thesis, Dept. Electr. Comput. Eng., Boise State Univ., Boise, ID, USA, 2012.

Marcus Pearlman (S'11) received the B.S. degree in electrical engineering from the University of Colorado, Boulder, CO, USA, in 2005, and the M.S. degree from Boise State University, Boise, ID, USA, in 2012, where he is currently pursuing the Ph.D. degree in electrical engineering.

His current research interests include microwave vacuum electron devices and computational science.

Tyler Rowe (S'09) received the B.S. degree in electrical engineering from Boise State University, Boise, ID, USA, in 2011, where he is currently pursuing the M.S. degree with the Electrical and Computer Engineering Department.

His current research interests include microwave vacuum electron devices.

Jim Browning (M'90–SM'08) received the B.S. and M.S. degrees in nuclear engineering from the University of Missouri-Rolla, Rolla, MO, USA, in 1983 and 1985, respectively, and the Ph.D. degree from the University of Wisconsin, Madison, WI, USA, in 1988.

He has been an Associate Professor with the Department of Electrical and Computer Engineering, Boise State University (BSU), Boise, ID, USA, since 2006. Prior to joining BSU, he was a Consultant of emission technology, as a Senior Development Engineer with PixTech, Inc., Boise, and Micron Technology, Inc., Boise. His current research interests include microwave vacuum electron devices and plasma propulsion.